University of Kent

Kent Academic Repository

Ghazanfari Holagh, Shahriyar, Abdous, Mohammad Ali, Rastan, Hamidreza, Shafiee, Mahmood and Hashemian, Mehran (2022) ***Performance analysis of micro-fin tubes compared to smooth tubes as a heat transfer enhancement technique for flow condensation.*** **Energy Nexus, 8 (100154). pp. 1-15.**

Downloaded from

https://kar.kent.ac.uk/97571/ The University of Kent's Academic Repository KAR

The version of record is available from

https://doi.org/10.1016/j.nexus.2022.100154

This document version

Author's Accepted Manuscript

DOI for this version

Licence for this version

CC BY-NC-ND (Attribution-NonCommercial-NoDerivatives)

Additional information

Versions of research works

Versions of Record

If this version is the version of record, it is the same as the published version available on the publisher's web site. Cite as the published version.

Author Accepted Manuscripts

If this document is identified as the Author Accepted Manuscript it is the version after peer review but before type setting, copy editing or publisher branding. Cite as Surname, Initial. (Year) 'Title of article'. To be published in *Title of Journal* , Volume and issue numbers [peer-reviewed accepted version]. Available at: DOI or URL (Accessed: date).

Enquiries

If you have questions about this document contact ResearchSupport@kent.ac.uk. Please include the URL of the record in KAR. If you believe that your, or a third party's rights have been compromised through this document please see our Take Down policy (available from https://www.kent.ac.uk/guides/kar-the-kent-academic-repository#policies).

Energy Nexus 8 (2022) 100154

Contents lists available at ScienceDirect

Energy Nexus

journal homepage: www.elsevier.com/locate/nexus

Full Length Article

Performance analysis of micro-fin tubes compared to smooth tubes as a heat transfer enhancement technique for flow condensation

Shahriyar Ghazanfari Holagh[a], Mohammad Ali Abdous[a,*], Hamidreza Rastan[b], Mahmood Shafiee[c], Mehran Hashemian[d]

[a] School of Mechanical Engineering, Iran University of Science and Technology, Tehran, Iran
[b] Department of Energy Technology, KTH Royal Institute of Technology, Stockholm SE-100 44, Sweden
[c] Group of Mechanical Engineering, School of Engineering and Digital Arts, University of Kent, Canterbury, United Kingdom
[d] Department of Mechanical Engineering, Faculty of Engineering, Urmia University, Urmia, Iran

ARTICLE INFO

Keywords:
Entropy generation analysis
Micro-fin tube
Entropy generation number
Heat transfer enhancement
Pressure drop
Condensation

ABSTRACT

Heat transfer enhancement techniques are accompanied by pressure drop amplification, detrimentally affecting their performance; entropy generation analysis is an effective approach to assess heat transfer enhancement along with resulting pressure drop. Current study investigates and compares the performance of micro-fin (as a passive enhancement technique) and smooth tubes during flow condensation (for R134a refrigerant) through conducting entropy generation analysis. First, the impact of geometrical and operating variables on pressure losses and heat transfer contributions to entropy generation and total generated entropy inside both types of tubes is examined. Then, the conditions at which the application of micro-fin tubes in lieu of smooth ones is justifiable and of superior performance are identified utilizing entropy generation number. The simulation results indicate that entropy generation enhances in the micro-fin tubes as tube diameter, mass velocity, vapor quality, and wall heat flux rise, and saturation temperature declines. The same is observed in the smooth tube except for the mass velocity; an increase in this parameter leads to a decreasing-increasing trend in entropy generation. Moreover, the entropy generation number results indicate that applying micro-fin tubes rather than smooth ones is justifiable, i.e., has better performance, at lower mass velocities and vapor qualities, but higher saturation temperatures and wall heat fluxes.

1. Introduction

Heat exchangers are commonly used in a wide range of cooling processes during which heat is transferred via condensation like refrigeration cycles, air conditioning systems, thermal cooling in chemical, pharmaceutical, and agricultural products, heat pumps, and so on [1,2]. Improving the performance of such components can remarkably reduce the costs (material, weight, and energy saving) and efficiency (energy and exergy efficiencies) of the cooling processes they are involved in Allahyarzadeh-Bidgoli et al. [3]. Hence, over the last decades, many passive heat transfer enhancement techniques (HTET) have been developed to enhance the thermal performance of heat exchangers without utilizing an external power source in such systems [4,5]. In essence, thanks to the complex geometry they have, passive HTETs can cause further improvements in heat transfer. In fact, such techniques influence two-phase flows behavior, phases' interaction, bubbles' behavior, void fraction, etc., resulting in lower thermal resistances, i.e., higher two-phase heat transfer coefficients (HTC) [6–8]. Nonetheless, these techniques ameliorate heat transfer at the cost of a significant growth in pressure drop, i.e., hydraulic losses, causing negative impacts on the exchanger's performance. In addition to the hydraulic losses, thermal losses can occur during condensation process if HTETs are applied within the ranges of geometrical and operating conditions at which heat transfer is not of its best performance, leading to depletion in the effectiveness of HTETs [9,10].

Micro-fin tubes are a common type of passive HTETs that can effectively enhance heat transfer while withstanding high pressures required by recently presented environmentally-friendly refrigerants like R134a. Thereby, they are frequently utilized in air conditioning and refrigeration systems and condensers [11]. However, as substantiated by numerous experimental studies, these tubes are not an exception to the above-discussed rules (thermal-hydraulic losses). Many researchers have experimentally investigated the characteristics of heat transfer and pressure drop for R134a flow condensation within micro-fin tubes. To mention a few, in a comparative experimental study, carried out by Nualboonrueng et al. [12,13], R134a flow condensation heat transfer co-

* Corresponding author.
E-mail address: m.a.abdous@gmail.com (M.A. Abdous).

https://doi.org/10.1016/j.nexus.2022.100154
Received 9 April 2022; Received in revised form 7 October 2022; Accepted 17 October 2022
Available online 18 October 2022
2772-4271/© 2022 The Author(s). Published by Elsevier Ltd. This is an open access article under the CC BY license (http://creativecommons.org/licenses/by/4.0/)

Nomenclature

A_C	cross-sectional flow area (m^2)
A_w	cross-sectional tube wall area per fin (m^2)
B_T	bottom thickness (mm)
B_w	bottom width (mm)
D_i	tube inner diameter (mm)
D_O	tube outer diameter (mm)
D_H	tube hydraulic diameter (mm)
D_t	fin tip diameter (mm)
L	length (mm)
e_f	fin height (mm)
N	number of fins
P	perimeter (m)
S_p	perimeter of one fin and channel
dz	element discretization (m)
G	mass velocity ($kg.m^{-2}.s^{-1}$)
$\dot{m}$	mass flow rate ($kg.s^{-1}$)
T	temperature (°C)
x	vapor quality
p	pressure (Pa)
q''	heat flux ($W.m^{-2}$)
$\dot{Q}$	heat transfer rate (W)
U	convective heat transfer coefficient ($W.m^{-2}.K^{-1}$)
h	specific enthalpy ($J.kg^{-1}$)
k	thermal conductivity ($W.m^{-1}K^{-1}$)
c_p	heat capacity ($kJ.kg^{-1}K^{-1}$)
Nu	nusselt number
Re	reynolds number
Pr	prandtl number
Fr	froude number
Bo	bond number
N_s	entropy generation number
X	martinelli parameter
s	specific entropy ($J.kg^{-1}K^{-1}$)
$\dot{S}'_{gen}$	total entropy generation rate per unit length ($W.m^{-1}.K^{-1}$)
$\dot{S}'_{gen-ht}$	entropy generation rate per unit length due to heat transfer ($W.m^{-1}.K^{-1}$)
$\dot{S}'_{gen-pd}$	entropy generation rate per unit length due to pressure drop ($W.m^{-1}.K^{-1}$)
$\dot{S}'_{gen-mt}$	total entropy generation rate per unit length for micro-fin tube ($W.m^{-1}.K^{-1}$)
$\dot{S}'_{gen-st}$	total entropy generation rate per unit length for smooth tube ($W.m^{-1}.K^{-1}$)

Greek symbols

ρ	density ($kg.\ m^{-3}$)
v	specific volume ($m^3.kg^{-1}$)
μ	dynamic viscosity ($Ns.m^{-2}$)
ε	void fraction
σ	surface tension ($N.m^{-1}$)
α	fin angle (degree)
β	fin spiral angle (degree)
γ	apex angle (degree)

Subscripts

ht	heat transfer
pd	pressure drop
in	inlet
l	liquid
sat	saturation
tp	two-phase
v	vapor
w	wall
eq	equivalent
Go	gas only

efficient (FCHTC) and pressure drop were compared for micro-fin and smooth tubes. The comparison revealed that the application of micro-fin tubes improves FCHTC by 10%–85%, but at the expense of a 10%–50% growth in pressure drop. Singh and Kukreja [11] experimentally evaluated the dominance of enhanced pressure drop over the enhanced R134 FCHTC in micro-fin tubes. It was found that compared to smooth tubes, micro-fin tubes enhance R134 FCHTC by 21%–82%, while causing 111%–156% higher pressure drop. The experimental study of Yildiz et al. [14] showed that R134a FCHTC in micro-fin tubes is nearly 2.2 times greater than smooth tubes.

Some researchers have also studied the impact of operating conditions on R134a flow condensation heat transfer and pressure drop characteristics in micro-fin tubes. For a wide range of operating conditions, R134a FCHTC in micro-fin tubes was experimentally examined by Li et al. [15]. The authors concluded that the HTC augments as mass velocity rises and condensation temperature declines. Diani et al. [16] performed a series of experiments to study R134a FCHTC and pressure drop in small diameter micro-fin tubes. The findings revealed that HTC incessantly goes up as the vapor quality grows, whereas the pressure drop first increases and then, decreases.

A comprehensive experimental study was conducted by Adelaja et al. [17–20] to assess the influence of flow conditions on micro-fin tubes' enhancement factor for R134a flow condensation. The results indicated that with increasing vapor quality, the enhancement factor becomes larger. Longo et al. [21] experimentally analyzed the sensitivity of R134a FCHTC and pressure drop to operating conditions inside micro-fin tubes. They found that frictional pressure drop is strongly sensitive to variations in vapor quality, mass flux, and saturation temperature, while the HTC shows a high sensitivity only to vapor quality and mass flux.

As the above reviewed experiments show, similar to other HTETs, in addition to the potential thermal losses due to the inappropriate selection of geometrical and operating conditions, the improvement achieved in FCHTC by applying micro-fin tubes is always accompanied by a pressure drop penalty, compromising the efficacy of such an enhancement technique. Thus, entropy generation analysis, as a practical and reliable approach, must be adopted to identify, assess, and quantify possible thermal-hydraulic losses, and also determine operating and geometrical conditions at which these losses are of low amounts, that is, micro-fin tubes are of the best performance [22].

The generated entropy during two-phase flows has been numerically analyzed by many researchers. To simulate entropy generation during subcooled flow boiling while neglecting pressure drop term, Collado [23] developed a one-dimensional entropy generation analysis model. The influence of design variables on hydraulic losses for flow boiling of R134a refrigerant inside smooth tubes was numerically studied using entropy generation analysis by Eskin and Deniz [24]. Revellin et al. [25,26] proposed innovative mathematical models to evaluate and compare entropy generation during diabatic saturated two-phase flows in enhanced and smooth tubes. The findings showed that the enhanced tube is of superior performance than the smooth tube at low mass velocities. Additionally, it was found that entropy generation grows as the oil concentration increases. Holagh et al. [22] and Abdous et al. [27–29] applied and adapted the mathematical model proposed by Revellin et al. [25,26] to conduct an entropy generation analysis of R134a flow boiling in twisted-tape, micro-fin, helically coiled, and smooth tubes. The authors of the mentioned studies also identified operating and geometrical ranges within which the enhanced tubes are of smaller entropy generation values, i.e., better performance, compared to the smooth tube.

Many studies have applied entropy generation analysis to assess possible thermal-hydraulic losses during the condensation process. Laminar film condensation taking place on an isothermal plate was analyzed from the entropy generation standpoint by Adeyinka and Naterer [30]. Li and Yang [31] performed an entropy generation analysis of free convection film-wise condensation occurring on an elliptical cylinder by developing two expressions. Using these expressions, they calculated and minimized the generated entropy. Dung and Yang [32] optimized the free convection of saturated vapor film-wise condensation on a horizontal tube via the second law of thermodynamics. It was deduced that the contribution of heat transfer to entropy generation varies as the square of Nusselt number. Adopting the same approach, the saturated vapor film condensation on an isothermal sphere was optimized by Tzeng and Yang [33]. It was found that entropy generating enhances as Brinkman and Rayleigh numbers increase. Esfahani and Modirkhazeni [34] investigated flow condensation irreversibility on an isothermal, horizontal, elliptical tube versus alterations in geometrical parameters and Brinkman and Reynolds numbers. Ye and Lee [35] developed an entropy generation model to design an optimal refrigerant circuit used in a fin-and-tube condenser. Flow condensation of nano-refrigerants within a smooth tube was analyzed experimentally by Sheikholeslami et al. [36] from entropy generation and exergy viewpoints. The results indicated that an increase in the concentration of nanoparticles causes enhancements in pressure drop and its contribution to entropy generation. Sheikholeslami and Ebrahimpour [37] proved that using Al_2O_3-water nanofluid alongside of multi-way twisted tape enhanced thermal performance of Linear Fresnel Reflector (LFR). Some geometrical factors such as number of wings (n_w), revolution (TR) and width (ER) of tapes have been studied by authors. Reduction in generated entropy has been studied during flow condensation by NaCl's particles injection. The authors [38] described that the condensation process on salt particles has a major impact on two-phase characteristics. The numerical approach for calculation of frictional and thermal irreversibility for thermal analysis of PTC with a wavy absorber pipe has been applied via employing finite volume method (FVM). The contours of temperature, velocity, volume concentration, and exergy loss were presented [39]. The numerical simulation of entropy generation rate for MED-TVC desalination system has been studied by Li et al. [40]. They found that heat transfer contribution to entropy generation held higher share respect to viscous dissipation.

R134a flow condensation performance in helically coiled tube-in-tube heat exchangers was comprehensively examined by Holagh et al. [9] and Cao et al. [41] using entropy generation analysis. These studies concluded that as the tube diameter, mass velocity, vapor quality, and wall heat flux rise and saturation temperature declines, entropy generation augments.

With respect to the literature survey, the performance of micro-fin tubes as a passive HTET and potential thermal-hydraulic losses detrimentally affecting their effectiveness have not been evaluated under R134a flow condensation conditions in the previous studies. Moreover, in the literature, to the best knowledge of the authors, there is almost no study that compares R134a flow condensation performance between micro-fin tubes and smooth ones. As a result, desirable geometrical and operating ranges for the use of micro-fin tubes rather than smooth tubes during condensation process are still undistinguished and questionable. On the other hand, as previously discussed, the identification of such conditions is a key to take full advantage of a HTET's capabilities like micro-fin tubes. Hence, to fill such gaps, this study aims at analyzing the entropy generated during of R134a flow condensation within both micro-fin and smooth tubes. In that regard, first, the influence of geometrical and operating conditions, encompassing tube diameter, mass velocity, vapor quality, saturation temperature, and wall heat flux, on entropy generation and therefore, thermal-hydraulic losses, is analyzed. Then, to determine the conditions at which micro-fin tubes are of superior performance compared to the smooth tube, entropy generation number (N_s) is compared between the tubes at different operating and geometrical conditions. Thus, for R134a flow condensation, the conditions at which applying micro-fin tubes in lieu of smooth tubes is justifiable from loss prevention perspective are obtained. Also, it is worth mentioning that the technique introduced and expounded in the present study can be adopted by engineers and designers to prevent thermal-hydraulic losses and detect favorable conditions for other HTETs (like micro-channels, dimple tubes, foam-filled tubes, surface enhancement techniques, etc.) during both flow condensation and flow boiling.

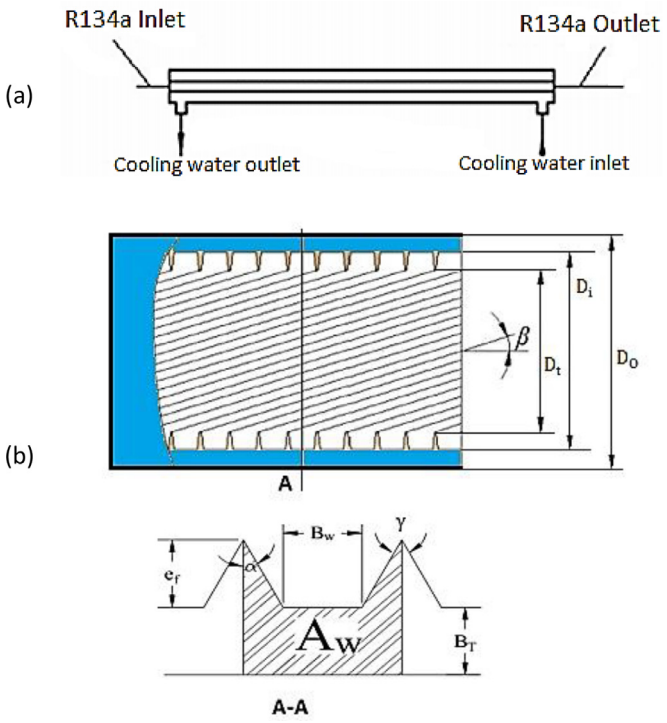

Fig. 1. Schematic views of (a) R134a and cooling water inlet and outlet, and (b) micro-fin tube interior structure (adopted from [29])

2. Entropy generation analysis

2.1. Physical model

Fig. 1a and b schematically show the refrigerant and cooling water inlet and outlet and the interior structure of a micro-fin tube with its important geometrical parameters, respectively. As can be seen, Saturated R-134a flows through the inner tube, while the cold water passes through the annular part. 4000 one-dimensional control volume elements (cells) are considered for both the micro-fin and smooth tubes, which satisfies grid independency as represented in Fig. 2a and b.

2.2. Mathematical model

Mathematical modeling is a key to have a better understanding of heat transfer problems [42,43,49]. To model entropy generation during R134a flow condensation within micro-fin and smooth tubes, a mathematical model, first developed by Revellin et al. [25,26], has been applied and adjusted in the present study. It is worth noting that the same model was applied by Holagh et al. [9,22], Cao et al. [41] and Abdous et al. [27–29] to simulate and evaluate thermal-hydraulic losses of R134a flow boiling and condensation inside enhanced tubes.

2.2.1. Assumptions

To simplify the simulations while keeping them reliable and accurate, below assumptions are considered.

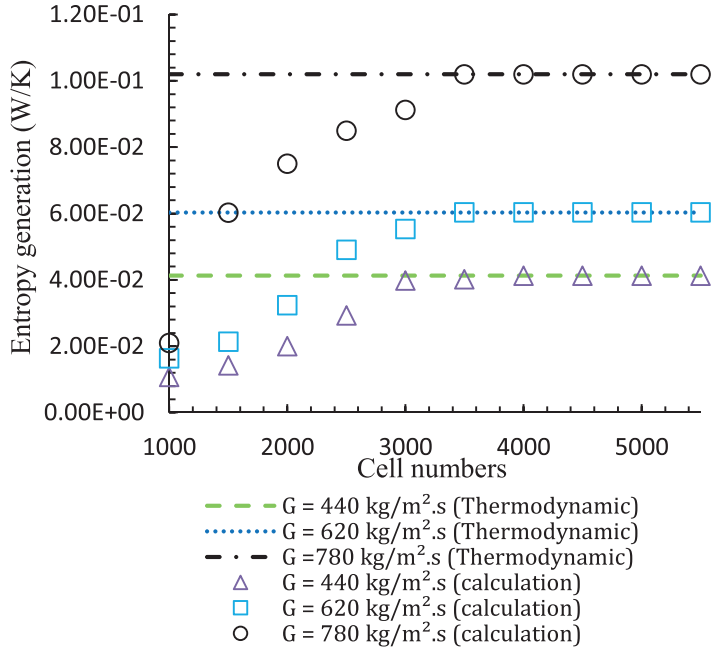

(a)

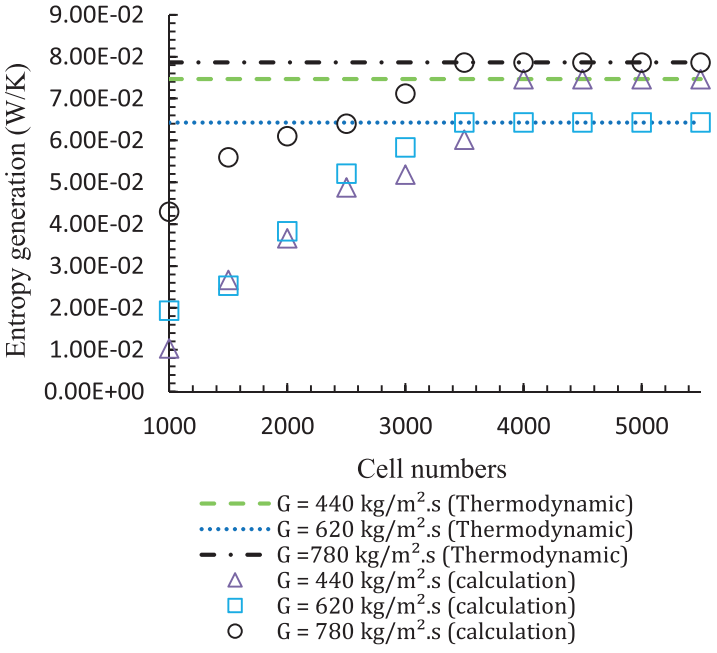

(b)

Fig. 2. (a) Grid independency examination and validation study for the micro-fin tube (Regarding Tables 2 and 3 as the input data), (b) Grid independency examination and validation study for the smooth tube (Regarding Table 2 as the input data for operating conditions and tube diameter and length of 9.52 mm and 2500 mm for the geometrical conditions, respectively)

- The operations are under steady-state conditions.
- Considering the second law of thermodynamics, entropy generation is calculated.
- The two-phase flows inside the tubes are supposed to be saturated and thus, the liquid and vapor phases' have the same temperatures.
- For vapor and liquid phases, pressure difference is supposed to be the same ($dp_v = dp_l$).
- For both vapor and liquid phases, dh is considered to be equal to Tds + vdp.
- As the tubes are horizontal, gravitational pressure drop term is negligible.
- Changes in kinetic and potential energies are negligible.
- Two-phase flow Nusselt number (Nu_{tp}) and multiplier ($\emptyset_l^2$) correlations proposed by Nualboonrueng et al. [12,13] are utilized to obtain HTC and frictional pressure loss, correspondingly.
- All the simulations are performed within the operating and geometrical ranges studied by Nualboonrueng et al. [12,13], that is, the utilized correlations are applicable and accurate for the simulations.

- One-dimensional grid is considered for both the micro-fin and smooth tubes. As the simulations are thermodynamics-based compute entropy generated within the tubes, the employment of one-dimensional grids is justifiable and appropriate.

2.2.2. Entropy generation calculation

The entropy generation rate per unit length ($\dot{S}'_{gen}$) for a control volume of length dz can be attained by Eqs. (1) and (2) utilizing the second law of thermodynamics [25]:

$$\dot{S}'_{gen}dz = d\left[\dot{m}_v s_v + \dot{m}_l s_l\right] - \delta\dot{Q}/T_w \tag{1a}$$

$$\dot{S}'_{gen}dz = \dot{m}d\left[x s_v + (1-x)s_l\right] - \delta\dot{Q}/T_w \tag{1b}$$

$$x = \dot{m}_v/\left(\dot{m}_v + \dot{m}_l\right) = \dot{m}_v/\dot{m} \tag{2}$$

Herein, $\dot{m}$ is mass flow rate, x represents vapor quality, s is specific entropy, T_W shows wall temperature, and $\delta\dot{Q}$ signify the differential heat transfer rate to the considered control volume. Subscripts w, l, and v correspondingly stand for wall, liquid, and vapor.

By noting $s_{lv} = s_v - s_l$, Eq. (1b) is simplified as:

$$\dot{S}'_{gen}dz = \dot{m}\left[s_v dx + x ds_v - s_l dx + (1-x)ds_l\right] - \delta\dot{Q}/T_w \tag{3a}$$

$$\dot{S}'_{gen}dz = \dot{m}\left[s_{lv} dx + x ds_v + (1-x)ds_l\right] - \delta\dot{Q}/T_w \tag{3b}$$

The term s_{lv} in Eq. (3b) is defined as [27]:

$$s_{lv} = h_{lv}/T_{sat} \tag{4}$$

It is noted that

$$dh_v = T_v ds_v + v_v dp_v \tag{5}$$

$$dh_l = T_l ds_l + v_l dp_l \tag{6}$$

Inserting s_{lv}, ds_v, and ds_l from Eqs. (4) to (6) into Eq. (3b) and assuming that $T_{sat} = T_v = T_l$ and $dp = dp_v = dp_l$ for flow condensation, Eq. (3b) is rearranged as Eq. (7a), or more simplified as Eq. (7b).

$$\dot{S}'_{gen}dz = \dot{m}\left[\frac{h_{lv}}{T_{sat}}dx + x\frac{\left(dh_v - v_v dp\right)}{T_{sat}} + (1-x)\frac{\left(dh_l - v_l dp\right)}{T_{sat}}\right] - \frac{\delta\dot{Q}}{T_w} \tag{7a}$$

$$\dot{S}'_{gen}dz = \frac{\dot{m}}{T_{sat}}\left[h_{lv}dx + x dh_v + (1-x)dh_l\right] - \frac{\delta\dot{Q}}{T_w} - \frac{\dot{m}\left[x v_v + (1-x)v_l\right]}{T_{sat}}dp \tag{7b}$$

Thus, $\dot{S}'_{gen}$ can be written in the form of Eq. (8), where dh_{tp} and v_{tp} are obtained using Eqs (9) and (10), respectively [25].

$$\dot{S}'_{gen}dz = \frac{\dot{m}}{T_{sat}}dh_{tp} - \frac{\delta\dot{Q}}{T_w} - \frac{\dot{m}v_{tp}dp}{T_{sat}} \tag{8}$$

$$dh_{tp} = h_{lv}dx + x dh_v + (1-x)dh_l \tag{9}$$

$$v_{tp} = x v_v + (1-x)v_l \tag{10}$$

Using the first law of thermodynamics and considering kinetic and potential energies negligible, $\delta\dot{Q}$ is attained as [25]:

$$d\dot{Q} = \dot{m}dh_{tp} \tag{11}$$

Ultimately, $\dot{S}'_{gen}$ is written by substituting Eq. (11) into Eq. (8) and doing some simplifications:

$$\dot{S}'_{gen} = \dot{m}\left[\frac{dh_{tp}}{dz}\left(\frac{1}{T_{sat}} - \frac{1}{T_w}\right) - \frac{v_{tp}}{T_{sat}}\frac{dp}{dz}\right] \tag{12}$$

Eq. (12) is separated into two parts:

$$\dot{S}'_{gen-ht} = \dot{m}\left[\frac{dh_{tp}}{dz}\left(\frac{1}{T_{sat}} - \frac{1}{T_w}\right)\right] \tag{13}$$

$$\dot{S}'_{gen-pd} = \frac{\dot{m}v_{tp}}{T_{sat}}\left(-\frac{dp}{dz}\right) \tag{14}$$

The first component, shown in Eq. (13), indicates the contribution of heat transfer to entropy generation (thermal losses), whereas the second component, given in Eq. (14), exhibits the contribution of pressure drop to entropy generation (hydraulic losses).

2.2.3. Entropy generation due to heat transfer

Heat transfer component of entropy generation ($\dot{S}'_{gen-ht}$) can help evaluate the thermal losses of R134a flow condensation within micro-fin and smooth tubes. In Eq. (13), the term $\frac{dh_{tp}}{dz}$, can be substituted with Eq. (15) using Eq. (16). In these equations, q, U, and P denote wall heat flux, HTC, and tube perimeter, respectively [42,44,45].

$$q'' = U\left(T_w - T_{sat}\right) = \delta\dot{Q}/Pdz = \dot{m}dh_{tp}/Pdz \tag{15}$$

$$\frac{dh_{tp}}{dz} = \frac{pq''}{\dot{m}} \tag{16}$$

Therefore, the simplified form of Eq. (13) is rearranged in the form of Eq. (17), indicating the contribution of heat transfer to entropy generation regarding $T_w - T_{sat} = \frac{q''}{U}$.

$$\dot{S}'_{gen-ht} = \frac{q''^2 P}{U T_w T_{sat}} \tag{17}$$

Note that wall temperature (T_w) is calculated utilizing HTC and wall heat flux as known parameters. Hence, to obtain the heat transfer contribution to entropy generation (thermal losses), first, the convective HTC (U) must be calculated. According to Nualboonrueng et al. [12], for R134a flow condensation inside micro-fin and smooth tubes, two-phase Nusselt number, Nu_{tp}, can be expressed in forms of Eqs (18) and (19), respectively.

$$Nu_{tp-microfin\ tube} = 0.079 Re_{eq}^{\ 0.652} Pr_l^{1.631} R_x^{-0.445} (Fr.Bo)^{0.033} \tag{18}$$

$$Nu_{tp-straight\ tube} = 0.003 Re_{eq}^{\ 0.997} Pr_l^{0.932} \tag{19}$$

Herein, Re_{eq}, Pr_l, R_x, Fr, and Bo represent equivalent Reynolds number, Prandtl number, geometrical parameters, Froude number, and Bond number, which are computed using Eqs (20)–(24), correspondingly.

$$Re_{eq} = Re_l + Re_v\left(\frac{\mu_v}{\mu_l}\right)\left(\frac{\rho_l}{\rho_v}\right)^{0.5} \tag{20}$$

$$Pr_l = \frac{Cp_l\mu_l}{k_l} \tag{21}$$

$$R_x = \left[\frac{2e_f N\left(1 - \sin\left(\frac{\gamma}{2}\right)\right)}{\pi D_t \cos\left(\frac{\gamma}{2}\right)} + 1\right]/\cos(\beta) \tag{22}$$

$$Fr = \frac{u_{GO}^2}{gD_t} \tag{23}$$

$$Bo = \frac{G\rho_l e_f D_t}{8\sigma N} \tag{24}$$

In Eq. (22), e_f, N, γ, β are fins' height, number, apex angle, and spiral angle, correspondingly. Moreover, in Eq. (23), u_{Go} denotes flow velocity when all the flow is considered to be in vapor phase.

Table 1
Constants for Eqs (41) and (42)

Property	a_0	a_1	a_2	a_3	a_4	a_5	Error (%)
p_v (10^5 Pa)	2.9283	0.10610	1.476×10^{-3}	9.127×10^{-6}	1.886×10^{-8}	-1.002×10^{-11}	0.03
h_{lv} (kJ/kg)	5.2912	-0.0038266	-1.918×10^{-5}	-1.366×10^{-7}	-1.419×10^{-9}	-1.186×10^{-11}	0.01
ρ_l (10^3 kg/m^3)	0.25819	-0.0025548	-8.450×10^{-6}	-5.340×10^{-8}	-6.130×10^{-10}	-4.306×10^{-12}	0.01
ρ_v (kg/m^3)	14.323	0.49951	7.608×10^{-3}	6.524×10^{-5}	-4.161×10^{-8}	-4.912×10^{-9}	0.56
μ_l (10^{-3} Ns/m^2)	-1.3047	-0.012721	1.307×10^{-5}	-3.630×10^{-7}	6.416×10^{-10}	4.390×10^{-12}	0.05
μ_v (10^{-7} Ns/m^2)	4.6756	0.0038342	-2.626×10^{-6}	8.789×10^{-8}	5.076×10^{-10}	6.183×10^{-12}	0.00
k_l (W/m-K)	-2.3865	-0.0047587	-4.998×10^{-6}	-1.537×10^{-7}	-7.550×10^{-10}	2.111×10^{-11}	0.02
k_v (W/m-K)	0.011516	0.00008689	1.232×10^{-7}	2.031×10^{-9}	3.669×10^{-11}	2.864×10^{-13}	0.02
σ (10^{-3} N/m)	2.4473	-0.012448	-5.950×10^{-5}	-4.064×10^{-7}	-4.528×10^{-9}	-3.336×10^{-11}	0.01
$c_{p,l}$ (kJ/kg-K)	0.29357	0.0020423	1.143×10^{-5}	7.946×10^{-8}	1.491×10^{-9}	1.678×10^{-11}	0.01
$c_{p,v}$ (kJ/kg-K)	-0.10828	0.0050590	1.604×10^{-5}	1.136×10^{-7}	2.312×10^{-9}	2.517×10^{-11}	0.02

2.2.4. Entropy generation due to pressure drop

Pressure drop contribution to entropy generation ($\dot{S}'_{gen-pd}$) cab be utilized to assess the hydraulic losses of R134a flow condensation within micro-fin and smooth tubes. In Eq. (14), the term $\frac{dp}{dz}$, exhibiting the total pressure drop per unit length, is divided into three parts as [46]:

$$\left(\frac{dp}{dz}\right) = \left(\frac{dp_F}{dz}\right)_{tp} + \left(\frac{dp_G}{dz}\right)_{tp} + \left(\frac{dp_A}{dz}\right)_{tp} \tag{25}$$

where, $(\frac{dp_F}{dz})_{tp}$, $(\frac{dp_G}{dz})_{tp}$, and $(\frac{dp_A}{dz})_{tp}$depict frictional, gravitational, and accelerational components of the total pressure drop, respectively. Since the investigated micro-fin and smooth tubes are horizontal, the gravitational term in Eq. (25) is neglected. The accelerational term can be calculated by

$$\left(\frac{dp_A}{dz}\right)_{tp} = G^2 \frac{d}{dz}\left[\frac{x^2}{\varepsilon\rho_v} + \frac{(1-x)^2}{(1-\varepsilon)\rho_l}\right] \tag{26}$$

where, ρ_l, ρ_v, G, and ε signify the density of liquid and vapor phases, refrigerant's mass flux, and void fraction, respectively.

For a vapor-liquid two-phase flow, the frictional pressure drop, $(\frac{dp_F}{dz})_{tp}$, is written as [13]

$$\emptyset_l^2 = \left(\frac{dp_F}{dz}\right)_{tp} / \left(\frac{dp_F}{dz}\right)_l \tag{27}$$

where $\emptyset_l^2$ and $(\frac{dp_F}{dz})_l$ are the two-phase frictional multiplier and the single-phase liquid pressure drop, respectively. $(\frac{dp_F}{dz})_l$is defined as [13]:

$$\left(\frac{dp_F}{dz}\right)_l = \frac{2f_l G^2 (1-x)^2}{D_H \rho_l} \tag{28}$$

where, f_l represents the single-phase liquid friction factor defined as [13]

$$4f_l = 1.325\left[\mathrm{Ln}\left(\frac{e/D}{3.7}\right) + \frac{5.74}{Re_l^{0.9}}\right]^{-2} \tag{29}$$

where Re_l is calculated by Eq. (30), in which μ_l and D_H denote liquid phase dynamic viscosity and the tube's hydraulic diameter, correspondingly.

$$Re_l = \frac{GD_H(1-x)}{\mu_l} \tag{30}$$

Applying the e/D relation (Eq. (31)) proposed by Cavallini et al. [47], Eq. (29) can be adjusted to attain single-phase liquid flow pressure drop during refrigerants condensation inside a micro-fin tube.

$$e/D = 0.18\left(\frac{e_f}{D_t}\right)(0.1 + \cos\beta) \tag{31}$$

In Eq. (31), e_f is the fin height, D_t is the fin tip diameter, and β is the fin spiral angle.

For a smooth circular tube, two-phase frictional multiplier ($\emptyset_l^2$) is expressed by the Lockhart-Martinelli correlation:

$$\emptyset_l^2 = 1 + \frac{C}{X} + \frac{1}{X^2} \tag{32}$$

where, C is a variable exhibiting two-phase flow condition; its value is different (between 5 and 20) at different flow conditions [48]. For R134a flow condensation inside micro-fin and smooth tubes, Nualboonrueng and Wongwises [13] suggested below equations for the two-phase frictional multiplier ($\emptyset_l^2$).

$$\emptyset^2_{l-microfin\ tube} = 1 + \frac{3.388}{X^{1.640}} \tag{33}$$

$$\emptyset^2_{l-straight\ tube} = 1 + \frac{5.705}{X^{1.711}} \tag{34}$$

Also, X denotes Martinelli parameter obtained from

$$X^2 = \left(\frac{dp_F}{dz}\right)_l / \left(\frac{dp_F}{dz}\right)_v \tag{35}$$

where, $(\frac{dp_F}{dz})_v$is the single-phase vapor pressure drop defined as:

$$\left(\frac{dp_F}{dz}\right)_v = \frac{2f_v G^2 x^2}{D_H \rho_v} \tag{36}$$

Herein, f_v depicts the single-phase vapor friction factor computed via [13]

$$4f_v = 1.325\left[\mathrm{Ln}\left(\frac{e/D}{3.7}\right) + \frac{5.74}{Re_v^{0.9}}\right]^{-2} \tag{37}$$

where Re_v is computed by Eq. (27), in which μ_v represents vapor phase dynamic viscosity.

$$Re_v = \frac{GD_H x}{\mu_v} \tag{38}$$

Utilizing Eq. (31) with Eqs (36)–(38), f_v and $(\frac{dp_F}{dz})_v$ are acquired. Then, X^2 is obtained using Eq. (35). The substitution of Eqs (28), (33), and (34) into Eq. (27), gives two-phase flow frictional pressure drop, $(\frac{dp_F}{dz})_{tp}$, inside the micro-fin and smooth tubes.

2.2.5. Flow conditions and geometrical parameters

The developed numerical code utilizes the below polynomial functions to obtain R134a thermo-physical properties [22]:

$$\text{property} = a_0 + a_1 T + a_2 T^2 + a_3 T^3 + a_4 T^4 + a_5 T^5 \tag{39}$$

$$\ln(\text{property}) = a_0 + a_1 T + a_2 T^2 + a_3 T^3 + a_4 T^4 + a_5 T^5 \tag{40}$$

Table 1 provides coefficients a_0 to a_5. Eq. (39) is employed to calculate p_v, ρ_v, and k_v, whereas Eq. (40) is applied to compute h_{lv}, ρ_l, μ_v, μ_l, k_l, σ, c_{pl} and c_{pv}.

In addition, according to Abdous et al. [29], the important geometrical parameters of a micro-fin tube, including tube inner diameter (D_i), fin tip diameter (D_t), fin angle (α), perimeter of one fin and channel taken perpendicular to the axis of the fin (S_p), cross-sectional tube wall area per fin (A_w), cross-sectional flow area (A_C), and hydraulic diameter (D_H) are calculated utilizing below relations.

$$D_i = D_o - 2B_T \tag{41}$$

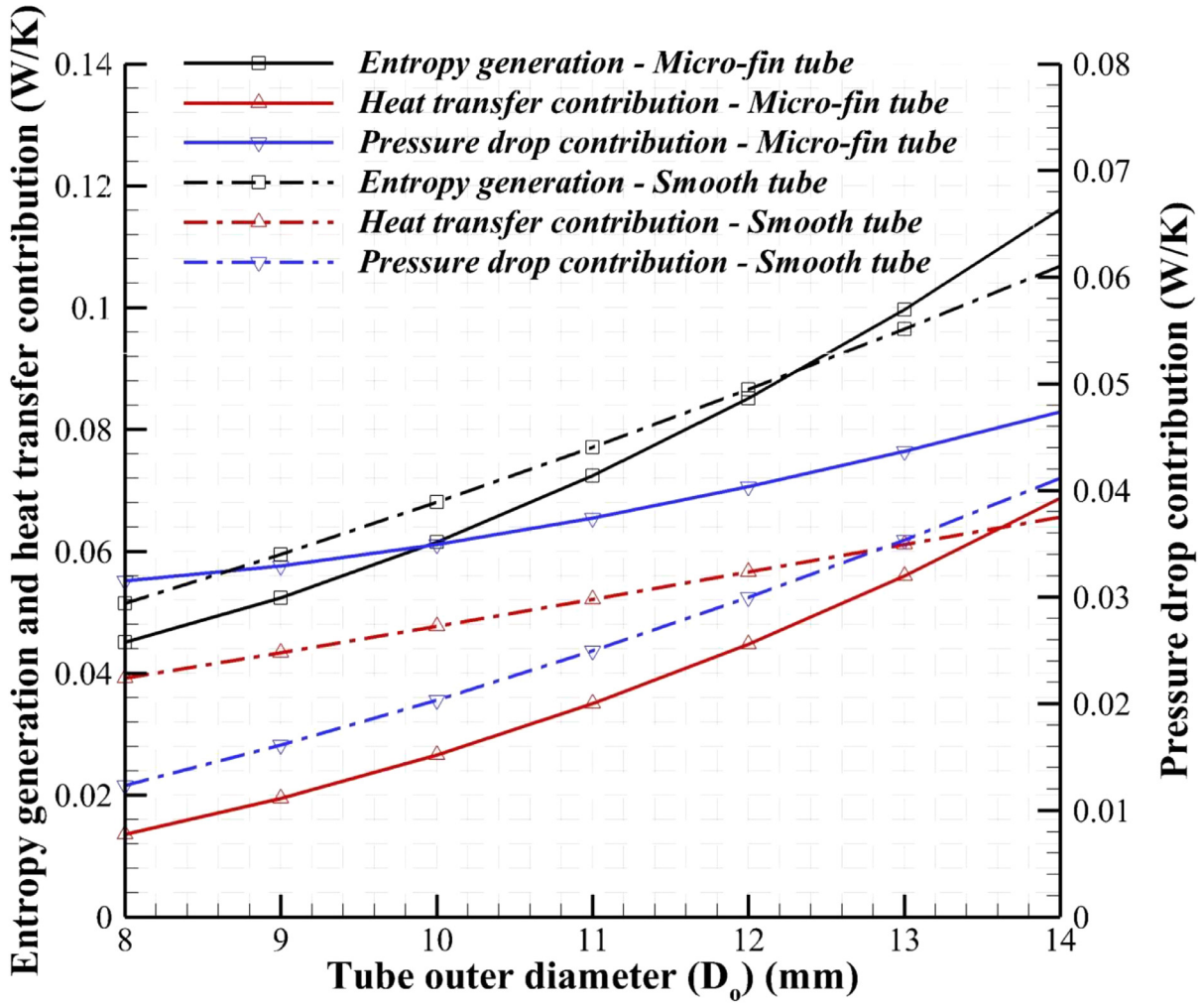

Fig. 3. Total entropy generation, heat transfer, and pressure drop contributions versus tube outer diameter for the micro-fin and smooth tubes at constant operating (Table 4) and geometrical (Table 3) conditions.

Table 2
Assumed operating conditions for validation purposes (Fig. 2a and b).

Variable	Unit	Value
Mass velocity (G)	$kg.m^{-2}s^{-1}$	440, 620, 780
Saturation temperature (T_{sat})	°C	40
Inlet vapor quality (x)	-	0.8
Wall heat flux (q″)	$W.\ m^{-2}$	20000

$$D_t = D_i - 2e_f \tag{42}$$

$$\alpha = \tan^{-1}\left(\frac{\frac{\pi D_i}{N} - B_w}{2e_f}\right) \tag{43}$$

$$S_p = B_w + \frac{2e_f}{\cos\alpha} \tag{44}$$

$$A_w = e_f^2 \tan(\alpha) + \left(2e_f \tan(\alpha) + B_w\right)B_T \tag{45}$$

$$A_C = \frac{\pi D_o^2}{4} - NA_w \tag{46}$$

$$D_H = \frac{4A_C \cos(\beta)}{NS_p} \tag{47}$$

2.2.6. Comparison approach

To compare the performance of the micro-fin and smooth tubes from an entropy generation perspective and subsequently, identify the ranges of operating and geometrical conditions within which the micro-fin tube is of superior performance, i.e., its applications is justifiable, entropy generation number (N_s) is used. This number, defined as the ratio of entropy generation rate in the micro-fin tube ($\dot{S}'_{gen-mt}$) to entropy generation rate in the smooth tube ($\dot{S}'_{gen-st}$), is given in Eq. (48).

$$N_s = \dot{S}'_{gen-mt}/\dot{S}'_{gen-st} \tag{48}$$

Note that the effectiveness of the micro-fin relative to the smooth tube can be determined by means of N_s. In essence, a value of $N_s < 1$ exhibits superior performance for the micro-fin tube with respect to the smooth tube, and vice versa.

2.3. Solution method

With regard to the mathematical model, introduced in the previous subsections), a MATLAB code was developed for the sake of entropy generation simulation within the tubes. Firstly, the tubes' geometries are discretized into several cells to an extent, where grid independency of the simulation results is attained. Then, the written code is being fed with the information related to the very first element including the initial pressure, initial temperature, mass flux and inlet vapor quality (mentioned in Table 4). Then, by considering the frictional two-phase pressure drop Eq. (27) for "dz" element, the pressure is obtained for

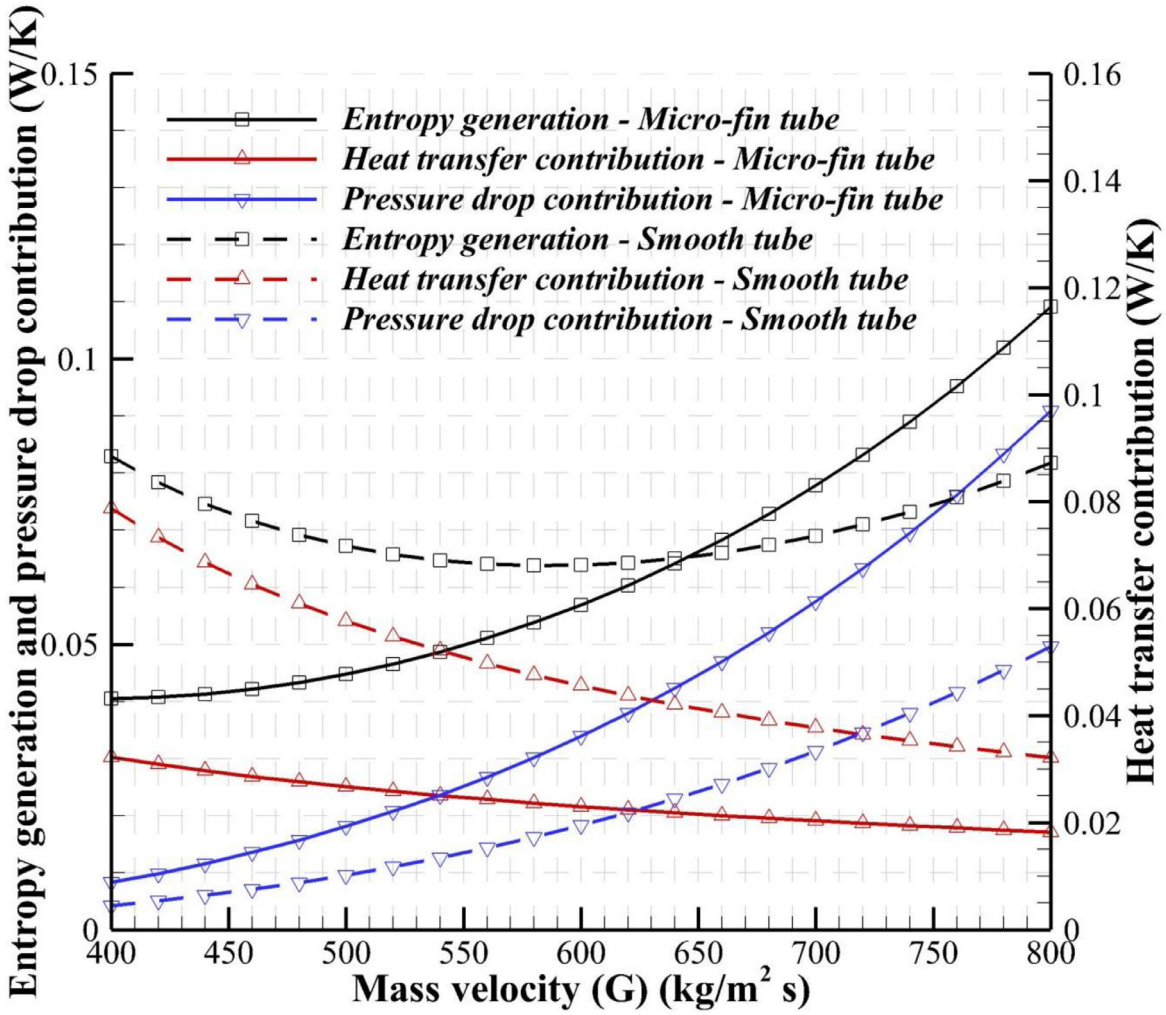

Fig. 4. Total entropy generation, heat transfer, and pressure drop contributions versus mass velocity for the micro-fin and smooth tubes at constant operating (Table 4) and geometrical (Table 3) conditions.

the second element. It should be noted that the total pressure drop could find by summing the frictional and accelerational shares in total pressure drop. Since, the saturation fluid temperature has direct dependency to pressure, the wall temperature is also found by solving Eqs. (15) and (16) by knowing heat transfer coefficient [12]. It should be mentioned that, the thermo-physical properties of the utilized working fluid (R134a) are calculated and employed in the mathematical model. By Knowing mentioned values for each element the measurement of total entropy generation and its contribution to pressure drop and heat transfer becomes feasible [29]. This process is proceeded to find all required information for each element. To assure the validity of the results, the total entropy generation values obtained from the simulations are compared with ones reported in thermodynamic charts. When the comparison shows that the difference between the results of the simulation and thermodynamic charts is lower than 10^{-5}, the simulation is considered accurate and stopped.

2.4. Validation study

Grid independency and validation assessments of the applied model and solution method for the micro-fin and smooth tubes are exhibited in Figs. 2a and b, respectively. As observable, the value of entropy generation calculated by the model reaches a constant value which is equal to that attained from thermodynamics charts after the point that corresponds to 4000 cells. That is, 4000 cells are sufficient for the considered geometries since the results are grid-independent and valid after this number.

3. Results and discussion

In this section, the simulation results are presented and discussed. First, the effect of operating and geometrical conditions on entropy generation and the contributions of heat transfer and pressure drop within both tubes are investigated and compared. Next to that, operating and geometrical ranges within which the micro-fin tube shows better performance are determined utilizing entropy generation number. Note that operating conditions presented in Table 4 together with geometrical conditions provided in Table 3 are utilized as input data; otherwise, conditions are as given.

3.1. Effect of geometrical and operating conditions

3.1.1. Tube diameter effect

For both micro-fin and smooth tubes, entropy generation and its components variations versus tube diameter, varying from 8 to 14 mm, are plotted in Fig. 3. From this figure, it is clear that for both tubes, as the diameter increases, heat transfer and pressure drop contributions and subsequently, total entropy generation rise significantly. In essence,

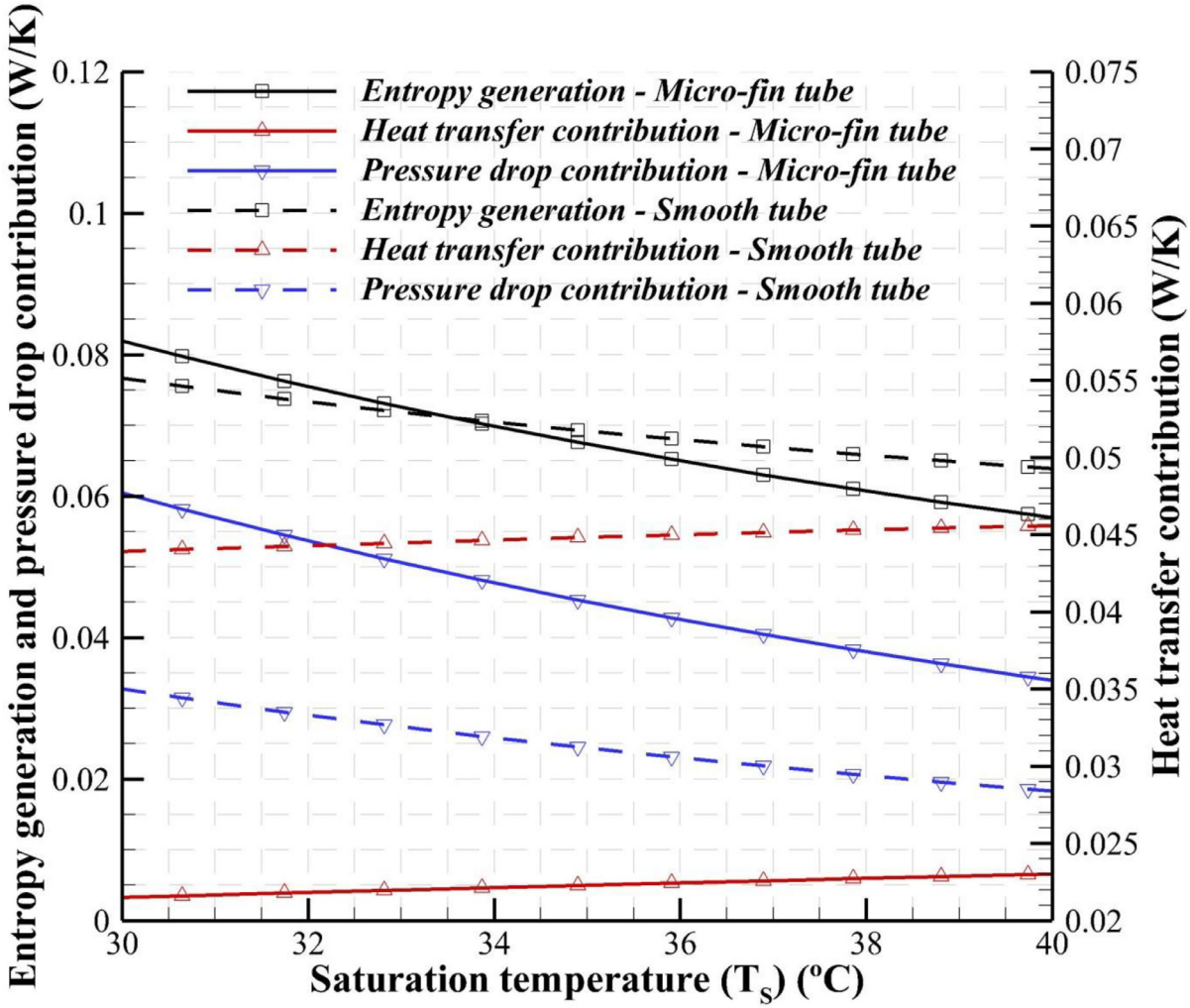

Fig. 5. Total entropy generation, heat transfer, and pressure drop contributions versus saturation temperature for the micro-fin and smooth tubes at constant operating (Table 4) and geometrical (Table 3) conditions.

Table 3
Assumed geometrical parameters for validation purposes and simulations.

Parameter	Value	Parameter	Value
L (mm)	2500	D_t (mm)	8.72
D_O (mm)	9.52	N	60
D_i (mm)	8.92	α (°)	26.225
e_f (mm)	0.1	β (°)	18
B_w (mm)	0.27	γ (°)	52.45
B_T (mm)	0.3		

the tubes' cross-sectional areas become larger as the tube diameter increases, resulting in increasing the mass flow rate of R134a flowing into the tubes at constant mass velocity. As a consequence, the difference between the saturation temperature and that of wall ($T_w - T_{sat}$) enhances and therefore, the heat transfer contribution to entropy generation grows. Meanwhile, when wall heat flux remains unchanged, mass flow rate becomes proportional to the tube diameter's second power, whereas the heat transferred from the wall to the flow is proportional to tube diameter. Thus, with increasing the diameter of the tube, the impact of the rise in mass flow rate on two-phase mixture density overcomes that of the heat transfer, leading to a decrease in two-phase mixture density [9,27,29]. Consequently, the two-phase mixture velocity increases at constant mass velocity, causing enhancements in pressure drop (hydraulic losses) and its contribution to entropy generation inside the tubes.

According to Fig. 3, it is also seen that the heat transfer contribution to entropy generation curves intersect each other at the tube diameter of 13.6 mm. At tube diameters lower than 13.6 mm, the higher HTC of the micro-fin tube compensates the increasing effect of the enhancement in $T_w - T_{sat}$ on entropy generation and therefore, this tube's heat transfer contribution to entropy generation becomes lower than that of the smooth tube. Nonetheless, for tube diameters greater than 13.6 mm, this is the enhancement in $T_w - T_{sat}$ that dominates the decreasing effect of the micro-fin tube's higher HTC on entropy generation, resulting in greater heat transfer contribution to entropy generation for this tube. As for the pressure drop contribution, it is observed that the micro-fin tube has the largest value within the whole considered range of tube diameter. This is because pressure drop is greater in the micro-fin tube than the smooth tube, particularly at smaller tube diameters, where the difference between the pressure drop contributions to entropy generation is bigger. Finally, due to the above-mentioned behaviors experienced by heat transfer and pressure drop contributions, the total entropy generation curves are seen to intersect each other at tube diameter of 12.4 mm. That is, before $D_o = 12.4$ mm, the micro-fin tube has lower total entropy

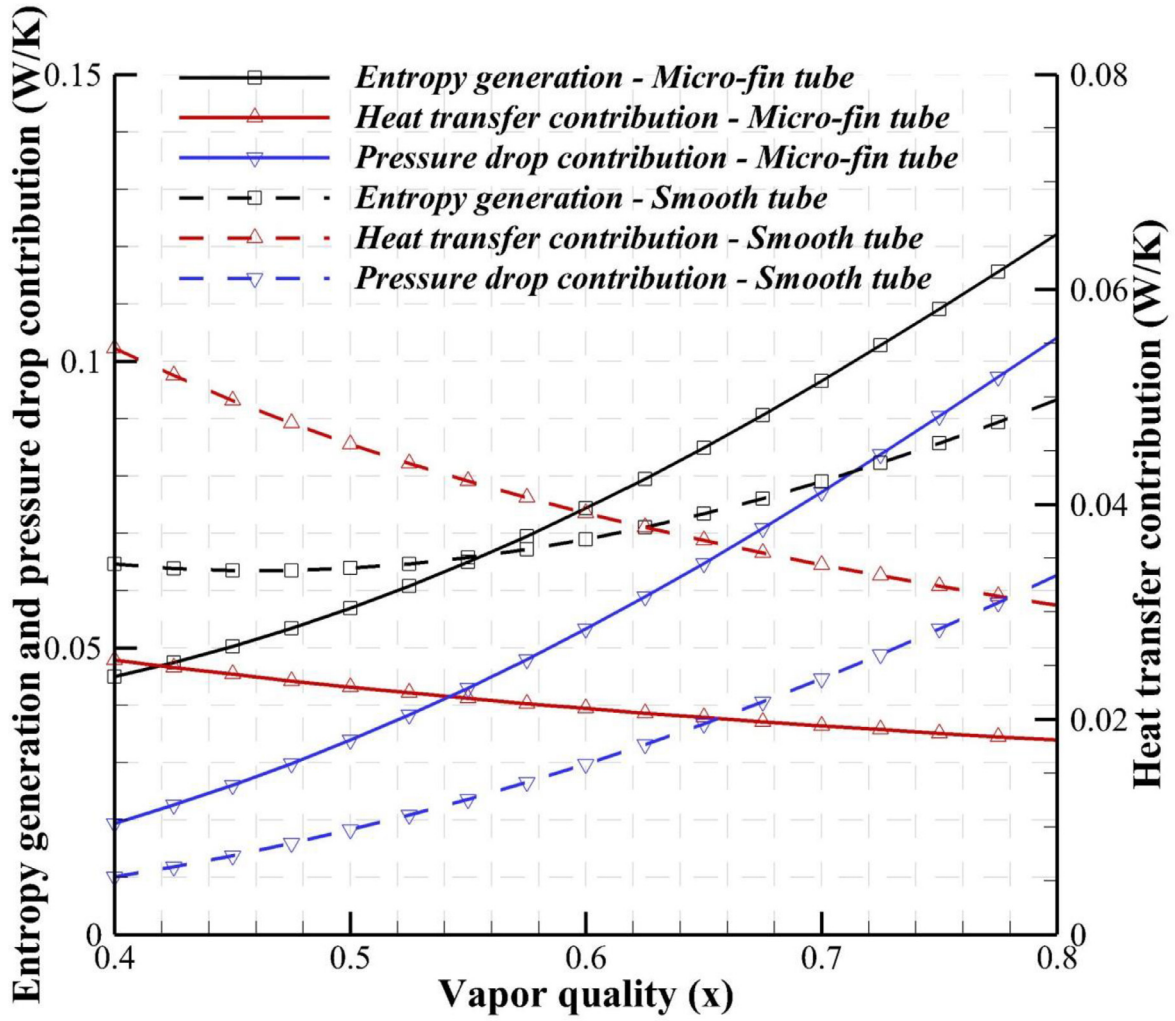

Fig. 6. Total entropy generation, heat transfer, and pressure drop contributions versus vapor quality for the micro-fin and smooth tubes at constant operating (Table 4) and geometrical (Table 3) conditions.

generation, while after this point; the smooth tube is of lower total entropy generation.

3.1.2. Mass velocity effect

Fig. 4 represents the effect of mass velocity, changing from 400 to 800 $kg.m^{-2}s^{-1}$ as same as assumed by Nualboonrueng et al's experimental tests [13,12], on entropy generation and its components for the micro-fin and smooth tubes. For both tubes, with increasing mass velocity, the heat transfer contribution reduces, whilst the pressure drop contribution augments. These are because both HTCs and pressure drops inside both tubes enhance respectively due to higher turbulence and greater frictional loss as a result of the increase in flow velocity when mass velocity rises at constant a cross-sectional area. For the smooth tube, the opposing trends experienced by heat transfer and pressure drop contributions cause a decreasing-increasing behavior in total entropy generation with a minimum value at mass velocity around 580 $kg.m^{-2}s^{-1}$. For the micro-fin tube, however, the total entropy generation steadily increases because of the dominance of the pressure drop contribution over the heat transfer contribution.

Since the micro-fin tube is of larger HTC and pressure drop, this tube shows larger pressure drop contribution and smaller heat transfer contribution to entropy generation within the entire range of studied mass velocity. However, as mass velocity goes up, the difference between the heat transfer contributions is seen to become smaller, whilst the difference between the pressure drop contributions grows. Looking at Fig. 4 meticulously, one can see that the total entropy generation curves reach the same value at the mass velocity of nearly 640 $kg.m^{-2}s^{-1}$ so that for $G \leq 640\ kg.m^{-2}s^{-1}$, the total entropy generation of the smooth tube is higher than that of the micro-fin tube, and vice versa.

3.1.3. Saturation temperature effect

The changes in entropy generation and relevant components versus saturation temperature, increasing from 30 to 50 °C, are illustrated in Fig. 5. In accordance with this figure, when the saturation temperature goes up, the total entropy generations and the pressure drop contributions reduce for both tubes, whereas the heat transfer contributions enhance. In essence, higher saturation temperatures mean higher saturation pressures, i.e., higher mixture densities or lower flow velocities under a constant mass velocity. The reduction in the flow velocity brings about a decrease in pressure drop and consequently, its contribution to entropy generation. On the other hand, such a decrease causes lower HTCs in both tubes and thus, increasing heat transfer contributions to entropy generation. Since the reduction in the pressure drop contributions is larger than the growth in the heat

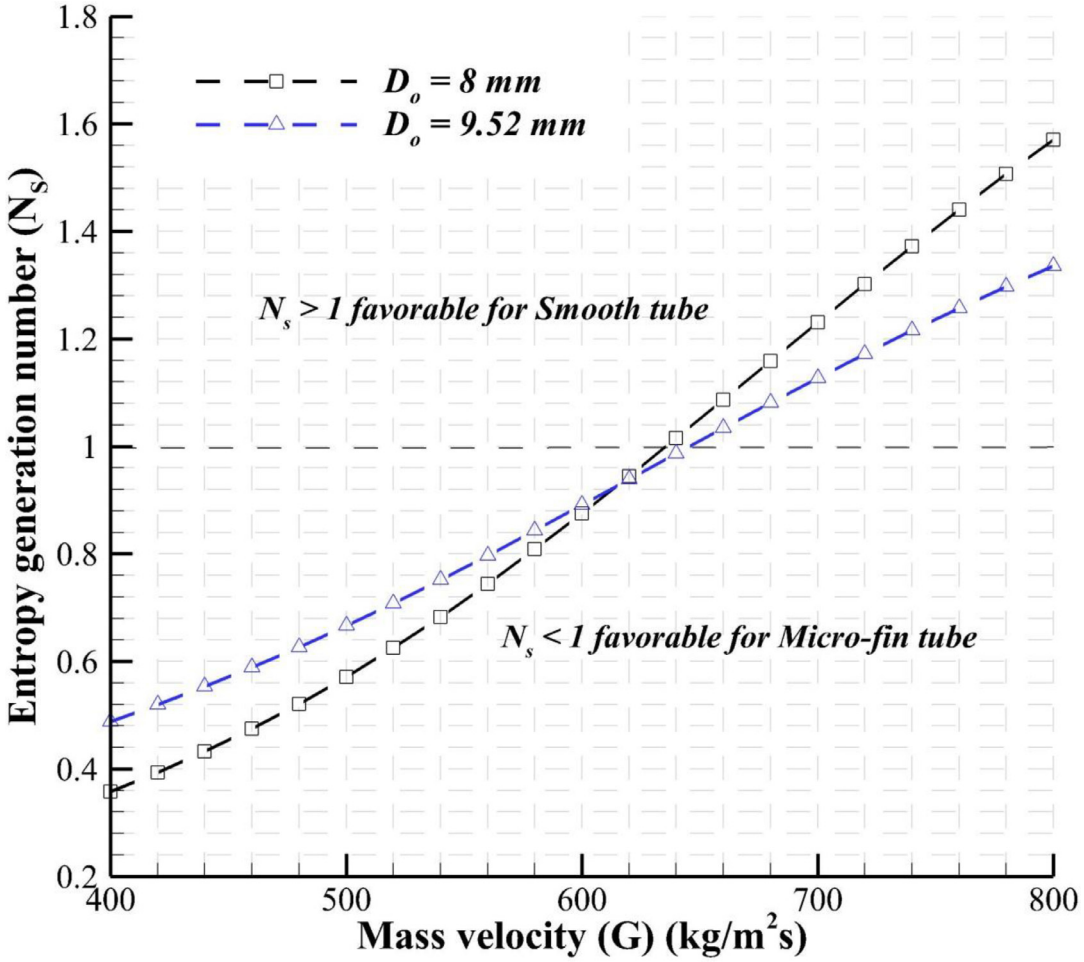

Fig. 7. N_s versus mass velocity for two different tube diameters (D_o = 8 mm and D_o = 9.52 mm), and geometrical and operating conditions reported in Tables 3 and 4, respectively.

transfer contributions, the total entropy generations decline for both tubes.

Compared to the smooth tube, the micro-fin tube witnesses a higher pressure drop as the saturation temperature rises. As well as this, the micro-fin tube is of higher HTC in comparison with the smooth one. Therefore, the pressure drop and heat transfer contributions to entropy generation are seen to be greater for the micro-fin tube within the whole range of saturation temperature. At the saturation temperature of 33.5 °C, the total entropy generation curves intersect each other; that is, when saturation temperature is lower than 33.5 °C, the smooth tube generates lower entropy, while for higher saturation temperatures, the micro-fin tube generates lower entropy.

3.1.4. Vapor quality effect

Fig. 6 exhibits the influence of vapor quality, changing from 0.4 to 0.8, on entropy generation and its components for both tubes. As the vapor quality increases, the heat transfer contributions show decreasing trends, while the total entropy generations and their pressure drop components demonstrate increasing trends. Under a constant mass velocity, two-phase mixture density reduces with increasing vapor quality, resulting in an enhancement in flow velocity. On the other hand, the higher the flow velocity is, the higher the HTCs and pressure drops are inside the tubes, causing larger pressure drop contributions, but lower heat transfer contributions. As the increase in the pressure drop contributions is greater than the decrease in the heat transfer contributions, the total entropy generations augment for both tubes.

Because of higher HTC and pressure drop within the micro-fin tube, for the entire range of vapor quality, this tube exhibits greater pressure drop contribution, but smaller heat transfer contribution to entropy generation compared to the smooth tube. A careful inspection of Fig. 6 shows that at vapor qualities less than 0.55, where the total entropy generation curve of the micro-fin tube falls behind that of the smooth one, the smooth tube generates more entropy, whereas at higher vapor qualities, this the micro-fin tube that generates more entropy.

3.2. Favorable operating conditions

Current subsection deals with identifying favorable geometrical and operating conditions for applying micro-fin tubes in lieu of smooth ones for R134a flow condensation. Such conditions, at which the micro-fin tubes exhibit superior performance compared to smooth tubes, are determined using entropy generation number (N_s). According to its definition, from an entropy generation perspective, when $N_s < 1$, the micro-fin tube demonstrates better performance than the smooth tube, and vice versa.

3.2.1. Mass velocity

Fig. 7 shows the variation of N_s against mass velocity for two different values of tube diameter. From this figure, it is conspicuous that for

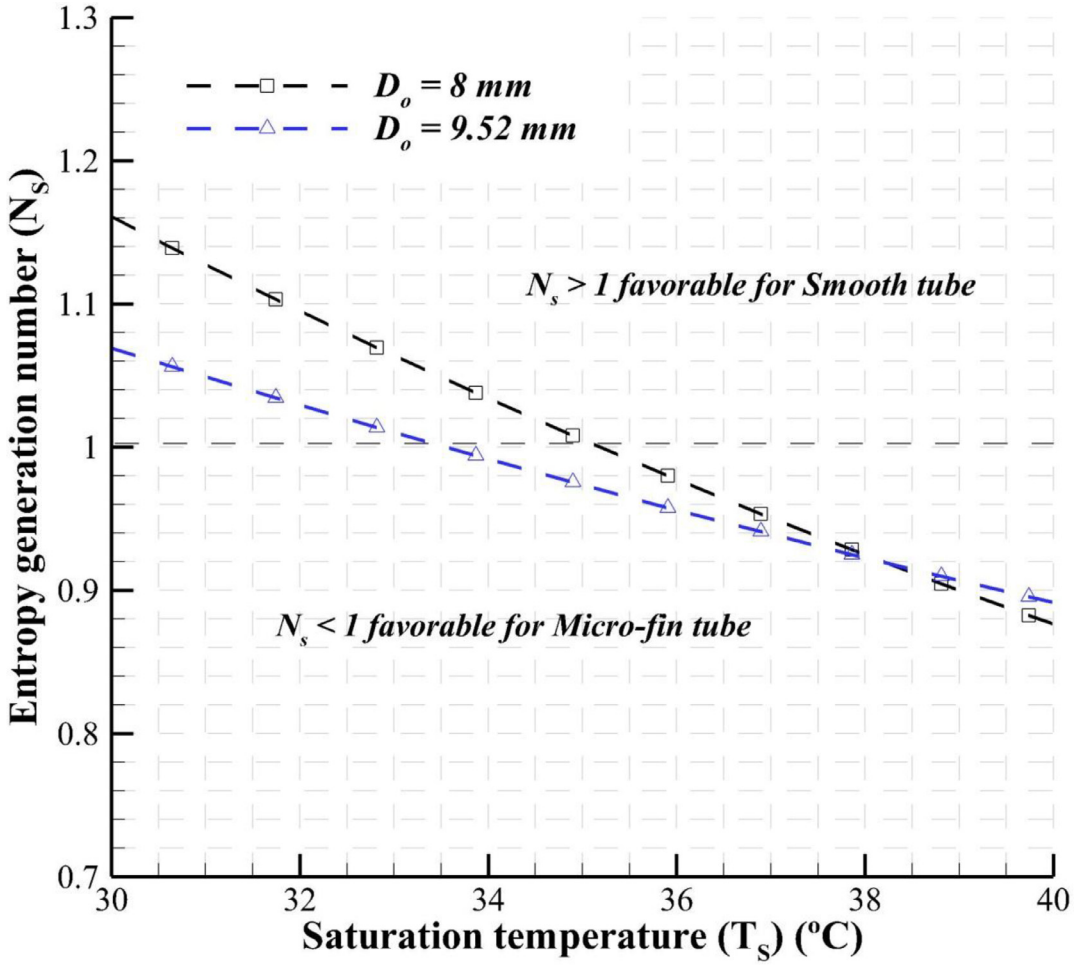

Fig. 8. N_s versus saturaion temperature for two different tube diameters (D_o = 8 mm and D_o = 9.52 mm), and geometrical and operating conditions reported in Tables 3 and 4, respectively.

both tube diameters, as the mass velocity rises, the N_s number increases. Simply put, with increasing mass velocity, the total amount of entropy generated by the micro-fin tubes becomes closer to and even exceeds that of the smooth tube, i.e., the lower the mass velocity is, the higher the justifiability of applying micro-fin tubes rather than smooth tubes is. In addition, the comparison between the N_s curves reveals that the greater the tube diameter is, the higher the mass velocity at which N_s crosses the line $N_s = 1$ is. Specifically speaking, for the micro-fin tube with $D_o = 9.52$ mm, the N_s value equals one at mass velocity of 640 $kg.m^{-2}s^{-1}$, but when the diameter reduces to 8 mm, the mass velocity at which the N_s number reaches unity declines by 10 $kg.m^{-2}s^{-1}$. Thus, for R134a flow condensation, the justifiability of employing micro-fin tubes within wider ranges of mass velocities can be accomplished at larger tube diameters.

3.2.2. Saturation temperature

The changes in N_s with saturation temperature are illustrated in Fig. 8 for two different values of tube diameter. With respect to this figure, with increasing saturation temperature, the N_s numbers of both tubes with different diameters reduce. That is, as the saturation temperature grows, the total amount of entropy generated by the micro-fin tubes approaches and even falls behind that of smooth tube so that the application of micro-fin tubes instead of smooth tubes becomes more justifiable at higher saturation temperatures. Moreover, by comparing the N_s curves, it is seen that the larger the tube diameter is, the lower the saturation temperature at which the entropy generation number crosses the line $N_s = 1$ is. For example, for the micro-fin tube with $D_o = 9.52$ mm, the N_s curve intersects the line $N_s = 1$ at the saturation temperature of 33.5 °C, but for the lower tube diameter ($D_o = 8$ mm), the saturation temperature at which the N_s becomes equal to unity increases to 35 °C. Thus, for R134a flow condensation, the justifiability of employing micro-fin tubes within wider ranges of saturation temperature can be accomplished at smaller tube diameters.

3.2.3. Vapor quality

Fig. 9 shows the variation of entropy generation number with vapor quality for two different values of tube diameter. Referring to this figure, it is obvious that an increase in vapor quality leads to enhancements in the N_s numbers of the micro-fin tubes with different tube diameters. In other words, with increasing vapor quality, the total amount of entropy generated by the micro-fin tubes reaches and even surpasses that of the smooth tube, i.e., the lower the vapor quality is, the higher the justifiability of employing micro-fin tubes rather than smooth tubes is. Furthermore, the micro-fin tube with lower tube diameter is seen to intersect the line $N_s = 1$ at lower vapor quality. For instance, for a reduction in the tube diameter from 9.52 to 8 mm, the vapor quality at which the N_s curve crosses the line $N_s = 1$ declines from 0.56 to 0.54. Thus, for R134a flow condensation, the vapor quality range, at which the utilization of micro-fin tubes brings about better performance, is widened by decreasing tube diameter.

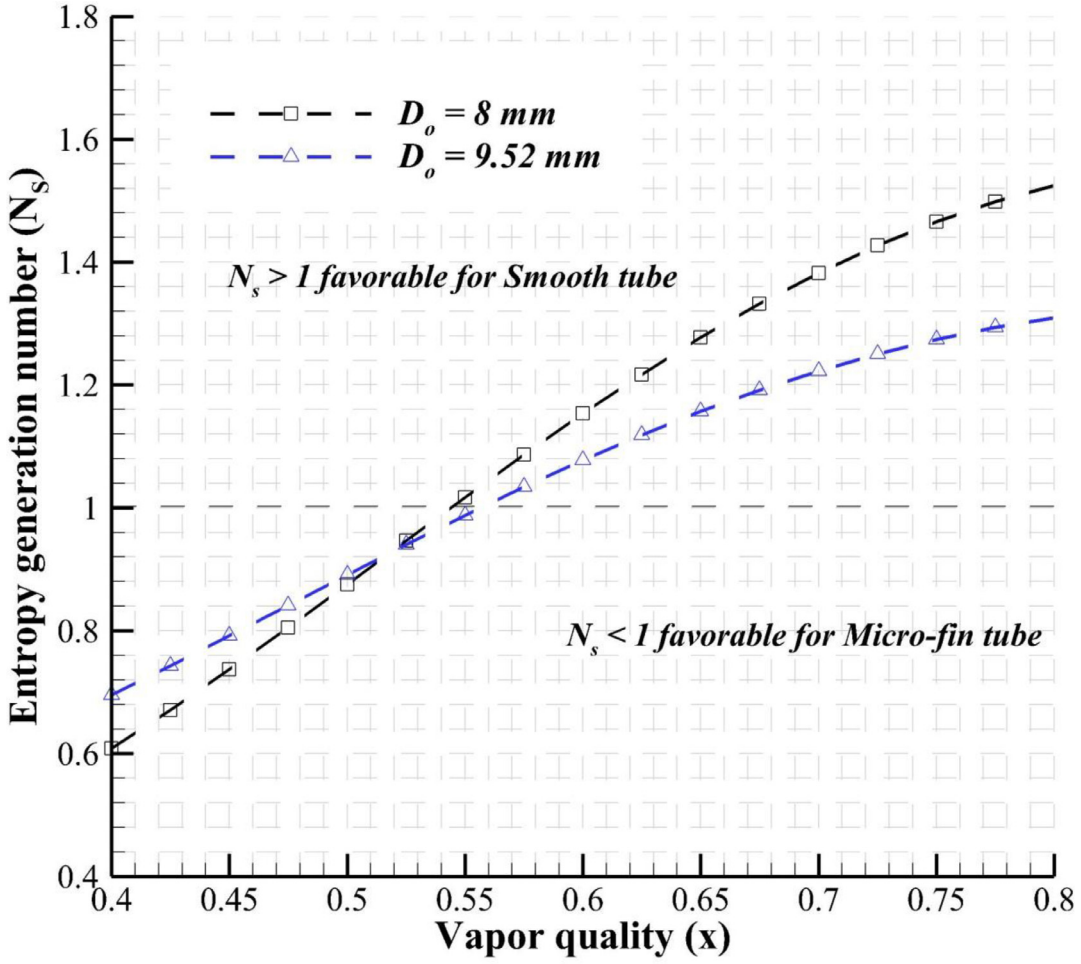

Fig. 9. N_s versus vapor quality for two tube diameters (D_o = 8 mm and D_o = 9.52 mm), and geometrical and operating conditions presented in Tables 3 and 4, respectively.

4. Conclusions

Entropy generation during R134a flow condensation within micro-fin and smooth tubes was analyzed and compared for wide ranges of geometrical and operating conditions. To this goal, a mathematical model was developed according to the second law of thermodynamics and coded in MATLAB. The influence of variations in geometrical parameters and operating conditions on entropy generation and its components due to heat transfer and pressure drop inside both tube types was studied. Also, the conditions in which superior performance of micro-fin tube is recognizable compared to the smooth tube from an entropy generation standpoint were identified. The main results of the study are summarized as follows.

- Within the ranges of experimental study of Naulboonrueng et al. [13,12], the geometrical parameter and flow conditions of the micro-fin tube are changed and compared to the smooth tube. These variations generally show larger pressure drop contribution, but smaller heat transfer contribution to entropy generation.
- Under constant flow conditions (Table 4), for both micro-fin and smooth, with increasing tube diameter, the pressure drop contribution to entropy generation enhance due to increse in mixture velocity while rising heat transfer components largely depends on increasing in the value of difference between the saturation temperature and wall ($T_w - T_{sat}$).
- Under constant geometrical parameters (Table 3), the higher heat transfer contribution to generated entropy with respect to pressure drop one at low mass flux (G) is attributed to lower velocity values. Increasing in fluid velocity causes gradual ascending trend in pressure drop share in generated entropy while heat transfer contribution falls slowly due to better heat transfer rate. The mixture velocity is a dominant factor in unveiling these trends. An increasing-decreasing trend explained above creates a minimum point in generated entropy of smooth tube. In contrast, in micro-fin tube, the growing trend in pressure drop share has such sufficient values at which has covered the reduction in heat share and finally leads to increasing trend in generated total entropy. Two entropy generation lines cross at 640 $kg.m^{-2}s^{-1}$ at which the value of $N_s = 1$ for 9.52 tube outer diameter.
- The pressure drop contribution to entropy generation decreases as saturation temperature increases under constant geometrical parameters (Table 3). Reduction in two-phase velocity as a consequence of increasing in mixture density plays a major rule in this regard. Due to dropping effect in two-phase velocity, the heat transfer contri-

Table 4
Assumed operating conditions for simulations.

Variable	Unit	Value
Mass velocity (G)	$kg.m^{-2}s^{-1}$	600
Saturation Temperature (T_{sat})	°C	40
Inlet vapor quality (x)	-	0.5
Wall heat flux (q″)	$W.\ m^{-2}$	20,000

bution to generated entropy follows opposite trend. Therefore, the total generated entropy illustrates the decline in trend as a result of higher increment in pressure drop contribution with respect to the heat transfer one. It worth noting that at the value of 33.5°C, for 9.52 mm tube outer diameter, the micro-fine and smooth tubes show the same value in generated entropy meaning $N_s = 1$.

- For both tube types, total entropy generation augments as vapor quality rises under constant geometrical parameters (Table 3). Increasing in vapor quality causes the dropping in mixture density leading to two-phase velocity increment at constant mass flux. As mixture velocity increases the pressure drop contribution to entropy generation mounts. Growing increase in two-phase velocity brings about the condition in which gradually better heat transfer rate becomes possible. Therefore, heat transfer contribution to entropy generation decreases. Since, the pressure drop contribution to generated entropy has the higher values than that of heat transfer one, thereby total generated entropy goes up steadily. The value of 0.55 in vapor quality demonstrates the value at which the entropy generation number equals to 1 for 9.52 mm tube outer diameter.
- From an entropy generation standpoint, in the range of experimental study performed by Naulboonrueng et al. [13,12], the employment of micro-fin tubes in lieu of smooth tubes can be justifiable, i.e., have superior performance, at lower mass velocities and vapor qualities, but higher saturation temperatures.
- The entropy generation number (N_s) is an important parameter in defining the favorable region using micro-fin tube and smooth one. Using its concept, one can easily find the favorable region in utlizing the specified geometry. The EGA shows that the desirable conditions for 8 mm and 9.52 mm tubes are different for both micro-fin and smooth tubes depending on flow conditions depicted in relevant (N_s) figures.
- Breifly, for assumped specified conditons (Table. 4) and tube outer diameter of 9.52 mm, less than the value of 640 $kg.m^{-2}s^{-1}$using the micro-fin tube would be preffered in contrast for higher than this value, there seems using smooth tube would be advisable. For 8 mm tube outer diameter, the turning point between preffered regions using micro-fin tube and smooth one takes lower values than 640 $kg.m^{-2}s^{-1}$.
- For 9.52 mm tube outer diameter and operting conditions in Table. 4, at the higher values of 33.5°C of saturation temperature, using micro-fin tube is recommended while less than this value the condition for utilizing smooth tube is advisable. For 8 mm tube outer diameter, the favorable regions using micro-fin tube becomes limited while wider regions are recommended when using 9.52 mm outer tube diameter.
- The EGA shows that, at the lower values of 0.55 for vapor quality, the micro-fin tube with outer diameter of 9.52 mm has a major superiority over smooth one while for 8 mm tube outer diameter, this turning point in vapor quality becomes lower. Detailed analysis demonstrates that the turning point moves to the right as tube diameter becomes larger. Therefore, employing micro-fin tube with higher tube diameter is a good choice with respect to the smooth one due to covering the wider vapor quality regions.

Declaration of Competing Interest

The authors declare that they have no known competing financial interests or personal relationships that could have appeared to influence the work reported in this paper.

Data Availability

The authors do not have permission to share data.

References

[1] X. Huang, J. Zhang, F. Haglind, Experimental analysis of hydrofluoroolefin zeotropic mixture R1234ze(E)/R1233zd(E) condensation in a plate heat exchanger, Int. Commun. Heat Mass Transf. 135 (2022) 106073, doi:10.1016/j.icheatmasstransfer.2022.106073.

[2] J.R. García-Cascales, F. Vera-García, J. Gonzálvez-Maciá, J.M. Corberán-Salvador, M.W. Johnson, G.T. Kohler, Compact heat exchangers modeling: condensation, Int. J. Refrig. 33 (2010) 135–147, doi:10.1016/j.ijrefrig.2009.08.013.

[3] A. Allahyarzadeh-Bidgoli, M. Mehrpooya, J.I. Yanagihara, Geometric optimization of thermo-hydraulic performance of multistream plate fin heat exchangers in two-stage condensation cycle: thermodynamic and operating cost analyses, Process Saf. Environ. Prot. 162 (2022) 631–648, doi:10.1016/j.psep.2022.03.088.

[4] E. Akbari, S.G. Holagh, H. Saffari, M. Shafiee, On the effect of silver nanoparticles deposition on porous copper foams on pool boiling heat transfer enhancement: an experimental visualization, Heat Mass Transf. 58 (2022) 447–466.

[5] M. Shamsaiee, S.G. Holagh, M.A. Abdous, H. Saffari, Experimental investigation of surface finishing technique impact on subcooled flow boiling heat transfer enhancement: sandpapering and sandblasting, Heat Mass Transf. (2022) 1–26.

[6] S.G. Holagh, M.A. Abdous, M. Shamsaiee, H. Saffari, An experimental study on the influence of radial pressure gradient on bubbles dynamic behavior in subcooled flow boiling, Therm. Sci. Eng. Prog. (2020) 16, doi:10.1016/j.tsep.2019.100468.

[7] S.G. Holagh, M.A. Abdous, P. Roy, M. Shamsaiee, M. Shafiee, H. Saffari, L. Vali, R. Andersson, An experimental investigation on bubbles departure characteristics during sub-cooled flow boiling in a vertical U-shaped channel utilizing high-speed photography, Therm. Sci. Eng. Prog. (2021) 22, doi:10.1016/j.tsep.2020.100828.

[8] M.A. Abdous, S.G. Holagh, M. Shamsaiee, H. Saffari, The prediction of bubble departure and lift-off radii in vertical U-shaped channel under subcooled flow boiling based on forces balance analysis, Int. J. Therm. Sci. 142 (2019) 316–331, doi:10.1016/j.ijthermalsci.2019.04.021.

[9] S.G. Holagh, M.A. Abdous, M. Shafiee, M.A. Rosen, Performance evaluation of helical coils as a passive heat transfer enhancement technique under flow condensation by use of entropy generation analysis, Therm. Sci. Eng. Prog. 23 (2021) 100914, doi:10.1016/j.tsep.2021.100914.

[10] M. Sheikholeslami, Numerical investigation of solar system equipped with innovative turbulator and hybrid nanofluid, Sol. Energy Mater. Sol. Cells 243 (2022) 111786, doi:10.1016/j.solmat.2022.111786.

[11] S. Singh, R. Kukreja, Experimental heat transfer coefficient and pressure drop during condensation of R-134a and R-410A in horizontal micro-fin tubes, Int. J. Air Cond. Refrig. 26 (2018) 1–16, doi:10.1142/S2010132518500220.

[12] T. Nualboonrueng, J. Kaewon, S. Wongwises, Two-phase condensation heat transfer coefficients of HFC –134a at high mass flux in smooth and micro-fin tubes, Int. J. Heat Mass Transf. 30 (2003) 577–590, doi:10.1016/S0735-1933(03)00086-1.

[13] T. Nualboonrueng, S. Wongwises, Two-phase flow pressure drop of HFC-134a during condensation in smooth and micro-fin tubes at high mass flux, Int. J. Heat Mass Transf. 31 (2004) 991–1004, doi:10.1016/j.icheatmasstransfer.2004.05.009.

[14] S. Yildiz, G. Duymaz, F. Ziegler, H. Auracher, Heat transfer during reflux condensation of R134a inside a micro-fin tube with different tube inclinations, Int. J. Refrig. 74 (2017) 425–434, doi:10.1016/j.ijrefrig.2016.11.004.

[15] Q. Li, L. Tao, L. Li, Y. Hu, S. Wu, Experimental investigation of the condensation heat transfer coefficient of R134a inside horizontal, Energies 10 (2017) 1–18, doi:10.3390/en10091280.

[16] A. Diani, M. Campanale, L. Rossetto, Experimental study on heat transfer condensation of R1234ze (E) and R134a inside a 4 . 0 mm OD horizontal microfin tube, Int. J. Heat Mass Transf. 126 (2018) 1316–1325, doi:10.1016/j.ijheatmasstransfer.2018.06.047.

[17] A.O. Adelaja, J.P. Meyer, D.R.E. Ewim, J. Dirker, Heat transfer, void fraction and pressure drop during condensation inside inclined smooth and microfin tubes, Exp. Therm. Fluid Sci. 109 (2019) 109905, doi:10.1016/j.expthermflusci.2019.109905.

[18] A.O. Adelaja, J. Dirker, P. Meyer, Condensation heat transfer coefficients and enhancements of R134a in smooth and microfin inclined tubes, Energy Procedia 158 (2019) 5299–5304, doi:10.1016/j.egypro.2019.01.644.

[19] P.K. Singh, K.B. Anoop, T. Sundararajan, S.K. Das, Entropy generation due to flow and heat transfer in nanofluids, Int. J. Heat Mass Transf. 53 (2010) 4757–4767, doi:10.1016/j.ijheatmasstransfer.2010.06.016.

[20] A.O. Adelaja, J. Dirker, J.P. Meyer, Experimental study of entropy generation during condensation in inclined enhanced tubes, Int. J. Multiph. Flow. 145 (2021) 103841, doi:10.1016/j.ijmultiphaseflow.2021.103841.

[21] G.A. Longo, S. Mancin, G. Righetti, C. Zilio, Saturated vapour condensation of R134a inside a 4 mm ID horizontal smooth tube : comparison with the low GWP substitutes R152a, R1234yf and R1234ze (E), Int. J. Heat Mass Transf. 133 (2019) 461–473, doi:10.1016/j.ijheatmasstransfer.2018.12.115.

[22] S.G. Holagh, M.A. Abdous, M. Shamsaiee, H. Saffari, Assessment of heat transfer enhancement technique in flow boiling conditions based on entropy generation analysis : twisted-tape tube, Heat Mass Transf. 56 (2020) 429–443, doi:10.1007/s00231-019-02705-y.

[23] F.J. Collado, The entropy balance for boiling flow, Fusion Eng. Des. 56–57 (2001) 199–203, doi:10.1016/S0920-3796(01)00259-9.

[24] N. Eskin, E. Deniz, Influence of design parameters on two-phase pressure drop and entropy generation during evaporation of refrigerants, in: Proceedings of the ECOS 2009 - 22nd International Conference on Efficiency, Cost, Optimization, Simulation and Environmental Impact of Energy Systems, 2009, pp. 159–168.

[25] R. Revellin, J. Bonjour, Entropy generation during flow boiling of pure refrigerant and refrigerant-oil mixture, Int. J. Refrig. 34 (2011) 1040–1047, doi:10.1016/j.ijrefrig.2011.01.010.

[26] R. Revellin, S. Lips, S. Khandekar, J. Bonjour, Local entropy generation for saturated two-phase flow, Energy 34 (2009) 1113–1121, doi:10.1016/j.energy.2009.03.014.

[27] M.A. Abdous, H. Saffari, H.B. Avval, M. Khoshzat, Investigation of entropy generation in a helically coiled tube in flow boiling condition under a constant heat flux, Int. J. Refrig. 60 (2015) 217–233, doi:10.1016/j.ijrefrig.2015.07.026.

[28] M.A. Abdous, S.G. Holagh, M. Shamsaiee, An evaluation of heat transfer enhancement technique in flow boiling conditions based on entropy generation analysis : micro-fin tube, in: Proceedings of The 4th International Electronic Conference on Entropy and Its Applications, 2017, pp. 1–9, doi:10.3390/ecea-4-05002.
[29] M.A. Abdous, H. Saffari, H. Barzegar Avval, M. Khoshzat, The study of entropy generation during flow boiling in a micro-fin tube, Int. J. Refrig. 68 (2016) 76–93, doi:10.1016/j.ijrefrig.2016.04.008.
[30] O. Adeyinka, G. Naterer, Optimization correlation for entropy production and energy availability in film condensation, Int. Commun. Heat Mass Transf. 31 (2004) 513–524, doi:10.1016/S0735-1933(04)00032-6.
[31] G. Li, S. Yang, Entropy generation minimization of free convection film condensation on an elliptical cylinder, Int. J. Therm. Sci. 46 (2007) 407–412, doi:10.1016/j.ijthermalsci.2006.06.007.
[32] S. Dung, S. Yang, Second law based optimization of free convection film-wise condensation on a horizontal tube, Int. Commun. Heat Mass Transf. 33 (2006) 636–644, doi:10.1016/j.icheatmasstransfer.2006.01.013.
[33] S.H. Tzeng, S.A. Yang, Second law analysis and optimization for film-wise condensation from downward flowing vapors onto a sphere, Heat Mass Transf. 43 (2007) 365–369, doi:10.1007/s00231-006-0119-5.
[34] J.A. Esfahani, M. Modirkhazeni, Entropy generation of forced convection film condensation on a horizontal elliptical tube, C. R. Méc. 340 (2012) 543–551, doi:10.1016/j.crme.2012.03.008.
[35] H. Ye, K. Lee, Refrigerant circuitry design of fin-and-tube condenser based on entropy generation minimization, Int. J. Refrig. 35 (2012) 1430–1438, doi:10.1016/j.ijrefrig.2012.03.013.
[36] M. Sheikholeslami, M. Darzi, Z. Li, Experimental investigation for entropy generation and exergy loss of nano-refrigerant condensation process, Int. J. Heat Mass Transf. 125 (2018) 1087–1095, doi:10.1016/j.ijheatmasstransfer.2018.04.155.
[37] M. Sheikholeslami, Z. Ebrahimpour, Thermal improvement of linear Fresnel solar system utilizing Al_2O_3-water nanofluid and multi-way twisted tape, Int. J. Therm. Sci. 176 (2022) 107505, doi:10.1016/j.ijthermalsci.2022.107505.
[38] G. Zhang, X. Wang, S. Dykas, M.A. Faghih Aliabadi, Reduction entropy generation and condensation by NaCl particle injection in wet steam supersonic nozzle, Int. J. Therm. Sci. (2022) 171, doi:10.1016/j.ijthermalsci.2021.107207.
[39] M. Sheikholeslami, Z. Said, M. Jafaryar, Hydrothermal analysis for a parabolic solar unit with wavy absorber pipe and nanofluid, Renew. Energy 188 (2022) 922–932, doi:10.1016/j.renene.2022.02.086.
[40] H. Li, X. Wang, H. Huang, J. Ning, A. Li, J. Tu, Numerical study on the effect of superheat on the steam ejector internal flow and entropy generation for MED-TVC desalination system, Desalination (2022) 537, doi:10.1016/j.desal.2022.115874.
[41] Y. Cao, M.A. Abdous, S. Ghazanfari Holagh, M. Shafiee, M. Hashemian, Entropy generation and sensitivity analysis of R134a flow condensation inside a helically coiled tube-in-tube heat exchanger, Int. J. Refrig. 130 (2021) 104–116, doi:10.1016/j.ijrefrig.2021.06.007.
[42] H. Fazeli, M.A. Abdous, H. Karabi, M. M, N. Esmaeili, Analysis of transient heat conduction in a hollow cylinder using duhamel theorem, Int. J. Thermophys. 34 (2013) 350–365.
[43] S.G. Holagh, F. Talati, M. Shamsaiee, Analytical solution of steady state heat conduction equations in irregular Domains with various BCs by use of Schwarz-Christoffel conformal mapping, Therm. Sci. Eng. Prog. 11 (2019) 8–18.
[44] G. Atefi, M.A. Abdous, A. Ganjehkaviri, N. Moalemi, An analytical solution of a two-dimensional temperature field in a hollow cylinder under a time periodic boundary condition using fourier series, Proc. Inst. Mech. Eng. Part C J. Mech. Eng. Sci. (2009) 223, doi:10.1243/09544062JMES1382.
[45] M.A. Abdous, N. Moallemi, Solution of two-dimensional transient heat conduction in a hollow sphere under harmonic boundary condition, Res. J. Appl. Sci. Eng. Technol. 7 (2014).
[46] S. Wongwises, M. Polsongkram, Condensation heat transfer and pressure drop of HFC-134a in a helically coiled concentric tube-in-tube heat exchanger, Int. J. Heat Mass Transf. 49 (2006) 4386–4398, doi:10.1016/j.ijheatmasstransfer.2006.05.010.
[47] A. Cavallini, D. Del Col, L. Doretti, G.A. Longo, L. Rossetto, Heat transfer and pressure drop during condensation of refrigerants inside horizontal enhanced tubes, Int. J. Refrig. 23 (2000) 4–25, doi:10.1016/S0140-7007(99)00032-8.
[48] H. Ito, Friction factors for turbulent flow in curved pipes, J. Basic Eng. 81 (1959) 123–132, doi:10.1115/1.4008390.
[49] M.A Abdous, H. Barzegar avval, P. Ahmadi, N. Moallemi, I. Dincer, et al., Analysis of transient heat conduction in a hollow sphere using Duhamel theorem, International Journal of Thermophysics 33 (1) (2012) 143–159, doi:10.1007/s10765-011-1136-2.